AERODYNAMIC CHARACTERIZATION OF A COMPARTMENT FIRE AS A FUNCTION OF ITS BEHAVIOR

MICKAEL COUTIN and JEAN-MICHEL MOST
Laboratoire de Combustion et de Détonique
UPR 9028 au CNRS - ENSMA
86961 Futuroscope Chasseneuil Cedex, FRANCE

ABSTRACT

An experimental setup is realized to study the behavior of a confined fire when the fire source is placed in combustion products trapped by a soffit, or located at the lower part of the rear wall of an enclosure. As a function of the source position, the flame, the heat release rate and the ventilation factor are drastically modified. In the first configuration, different flame behaviors are identified corresponding to jet flames, horizontal flames on the whole room surface at the level of the soffit, or extinction. In the second one, the wall fire interacts with the burnt gases close to the ceiling. The outwards hot smoke layer at the aperture always occupies one third of the open height. Based on the analysis of Babrauskas et al [1], a two zones hydrostatic model is developed, and a relation between the input air mass flow rate entering the room, the ventilation factor F_v and the heat release rate $\dot{Q}$ is obtained : $\dot{m}_{air} = f(F_v^{2/3}\dot{Q}^{1/3})$. For a fixed heat release rate, $\dot{m}_{air}$ only depends on the ventilation factor but stays independent of the flame structure in the room. This relation corroborates the experimental data and the theoretical analysis to results available in the literature and can be used to model for the structure of such flames.

KEYWORDS: compartment fire, under-ventilated flames, heat release rate, ventilation factor, flame behavior, two zones hydrostatic model.

INTRODUCTION

Since the fifties, the aerodynamic characterization of compartment fires are extensively studied for fire sources on the ground [1-9] and an exhaustive bibliography is available in the reviews of Babrauskas [2], Drysdale [3], or Karlsson [4]. These room fire studies mainly concern the fire growth of small sources, the toxic products and smoke generation, and the characteristic time for a potential transition to flashover. The development the fire is strongly linked to the combustion parameters, the location of the fuel material, the air mass flow rate feeding the combustion, and the thermal properties of the environment. Moreover, the geometry and the scale of the compartment, and the air supply characteristics can play an important role in the fire growth period [5]. Kawagoe

[6] had introduced the ventilation factor taking into consideration the aperture shape. Quintiere [7] gives a similar conclusion to that of Gross [8], on PMMA slabs, and show that for small widths of the opening, the fuel pyrolysis rate increases with the ventilation factor as long as the mass oxygen fraction is sufficient ; for larger openings, the mass loss depends on the fuel surface and on the thermal radiation, independently of oxygen excess. An extensive bibliography on entrainment rate in flame can be found in Dembsey et al [9].

For certain scenarios, the heat source is not placed on the floor, but either in the stratified vitiated upper zone containing mainly combustion products trapped by the soffit, or at the rear wall of the compartment ; the fire becomes under ventilated. Such an environment is now studied to identify the behaviors as a function of the heat release rate, the room geometry through soffit height, the heat source location, and to characterize the aerodynamic flow.

EXPERIMENTAL SETUP

Experimental Apparatus

The fire behavior in a compartment is investigated (Fig. 1). In order to separate the pyrolysis mass flow rate of a fuel solid surface from both the heat feedback from flame and hot body radiation to the solid surface, the degradation of the material is simulated by the injection of propane through the bronze porous surface of a flat burner [10].

Enclosure

The internal dimensions of the enclosure are 0.62 m in depth, 0.85 m in height and 0.41 m in width. A soffit (0.19 or 0.34 m), topping the room aperture, confines hot gases in the upper compartment region. The walls, ceiling and floor are insulated by 50 mm width Kerlane type ceramic fibers (thermal diffusivity 10^{-6} m^2/s) to minimize the heat losses. Lateral windows can replace the adiabatic walls in order to observe the structure and behavior of the flame. The walls of the lower room region are water cooled at 65°C.

Burners

Two porous burner types are separately used according to the studied configurations.

1/ For the fire source located in the upper vitiated zone, a water-cooled horizontal circular porous burner (0.062 m in diameter) is used. This burner can be moved up and down in the whole room volume by stepping motors. The burner is maintained in the center of the enclosure ($X_{bur.}$ = 0.310 m and $Z_{bur.}$ = 0.205). The thermal input is in the 1 to 21 kW range corresponding to a Froude number between $2.6 \ 10^{-5}$ and $1.42 \ 10^{-2}$. These fuel mass flow rates correspond to thermal input powers per unit compartment volume of 4.1 to 95.5 kW/m^3, which are representative of real fires ($\cong 3 \ MW$ for a standard test volume of 75 m^3).

2/ For the configuration of the permanently ventilated fire located at the rear of a compartment, a water-cooled vertical rectangular porous burner (0.40 m x 0.50 m) is used. Four propane mass flow rates are studied corresponding to the heat release $\dot{Q}$ of 18, 27, 36 and 45 kW, (mass transfer number B of 0.18, 0.28, 0.37 and 0.46). The Grashof number of the system is of the order of 10^{11}, so, the flow is strongly driven by buoyancy forces.

Diagnostic Techniques

Laser Tomography (outward hot gas thickness at the aperture)

The thickness of the outward flow of hot gas under the soffit is determined by laser tomography (Fig. 1.b). The entrance flow is seeded with incense smoke {smoke generator (1), air supply (2) and four cones of dispersion (3). A Nd-YAG laser (1) is coupled with an optical system (2) to form a vertical laser sheet. An intensified video camera (6), equipped with an interferential optic filter (5) centered on the laser wave length (532 nm), records the Mie scattering of lighted incense particles}. A statistical image processing on 500 uncoupled frames (7), including a correction of parallax deformations, gives a mean flow image and the output hot gas thickness at the aperture under the soffit.
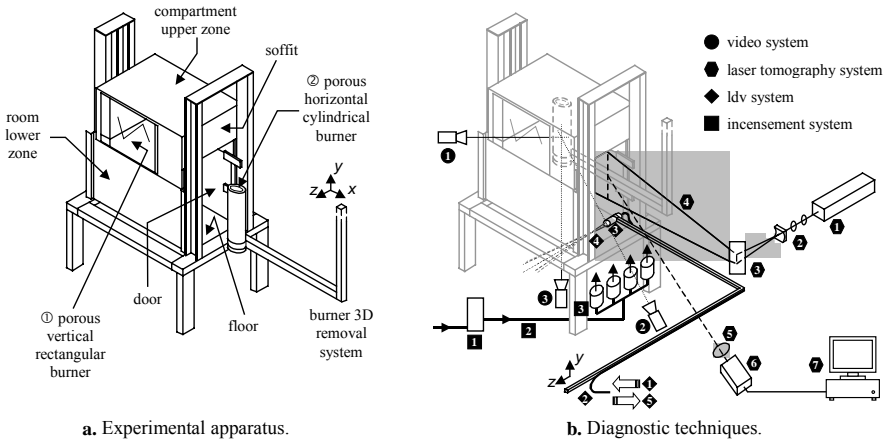

a. Experimental apparatus.   **b.** Diagnostic techniques.

Fig. 1. Experimental setup schemes.

Laser Doppler Velocimetry (input air velocity in the room at the door level)

To determine the fresh air mass flow rate, seeded with incense particles, entering the enclosure, the input air velocity is measured by Laser Doppler Velocimetry -LDV- system. This system is composed by a 5 W Argon Ion laser, a Bragg cell, a color separator (1), optical fibers (2) and an emission head (3). The measurement volume (4), obtained by the beams convergence, has a diameter of 0.03 mm and a length of 0.32 mm. The Doppler signal is detected by photomultipliers in back scattering mode. The Doppler signal is processed by a Burst Spectrum Analyzer (5). A statistical processing is made on 10 times 1024 uncorrelated instantaneous velocities in order to access to the mean incoming velocity, u, and air mass flow rate.

FLAME BEHAVIOR IDENTIFICATION

Three CCD cameras record spontaneous emission of the flame. The video recording is processed to identify and classify the flame behaviors. The test working conditions are the fire source position (burner - ceiling distance: $H_{bur.}$), the characteristics of the containment (soffit height: $H_{sof.}$) and the burner thermal input power $\dot{Q}$. The flame behavior is described for each study configuration (Fig. 2.).

1/ Fire Source in the Vitiated Upper Zone of the Compartment

The fire behavior is observed for different burner positions in the upper hot gases zone, for different thermal powers and the two soffit heights. Nine behaviors are observed [12].

1. Permanent Jet Flame (Fig.2 A)

For burner positions in the lowest region, the air mass flow rate available in the reactant diffusion zone is sufficient to completely, or partly, oxidize the hydrocarbon injected through the burner surface. Depending on $\dot{Q}$, the flame impinges by the ceiling surface, is deflected and interacts in the hot vitiated zone and flows towards the aperture.

2. Cyclic Flame (Fig. 2 B)

The first behavior of the cycle flame corresponds to a jet flame. Few seconds later, the flame decreases drastically in height and its color turns blue. The tip of the narrow flame, attached on the burner surface, moves to the aperture and flows at the hot and cold zone interface. After a short delay, the flame covers the whole surface at the soffit level. At the last step of the cycle, a puff of flame is convected out the compartment. The phenomenon lasts about 15 seconds.

During the cycle, the combustion efficiency, due to a lack of fuel at the hot and cold zone interface, decreases while the fuel gas is accumulated in the upper zone. The convective motion decreases and flame takes a blue color. When the hydrocarbon radical concentration reaches a threshold, a global combustion starts; the heat release induces the thermal expansion of the gases that are ejected outside.

3. Permanent Cloudy Flame between Burner and Aperture (Fig. 2 C)

For burner positions over the soffit level and the highest $\dot{Q}$ values, the flame leaves the burner surface. The blue-yellow cloud of flame, attached at the burner body, stretches towards the aperture. A thermal steady state is rapidly reached, the fuel is entirely oxidized inside of the compartment.

4. Ghosting Flame (Fig. 2 D)

For burner positions close to the ceiling, a very unstable blue flame is observed few millimeters under the soffit level at the interface between hot and cold zones and follows over the whole horizontal compartment surface. The instability of the phenomenon is attributed to the under-ventilation of the fuel rich upper region.

5. Yellow Interface Flame (Fig. 2 E)

For higher $\dot{Q}$ values and burner inside the vitiated region, large-scale yellow structures of flame covers the whole room surface few millimeters under the soffit bottom. A part of the hydrocarbon burns outside of the enclosure. The turbulence is amplified by the flame impingement on the ceiling and by the formation of a counter vortex in the upper corner.

6. Jet Flame and Cloud of Flame (Fig. 2 F)

For higher input powers, the jet flame impinges the ceiling and structures of flame flies in the vitiated region. The fuel is not completely oxidized in the diffusion flame, but burns in flamelet structures in the hot fuel rich zone.

7. Clouds of Flame with Sporadic Flame Motion in the Enclosure (Fig. 2 G)

For higher heat release $\dot{Q}$ values and burner locations close to the soffit level, a yellow-blue flame is stabilized in the wake of the burner to the aperture, and moves periodically as a counter flow to the rear of the enclosure. Depending on the motion velocity, the local equivalent ratio and temperature, fuel gases can be ignited behind the burner.

8. Interface Yellow-Blue Flame

This behavior is close to regime 5 for lower burner positions. It shows an heterogeneous flame color, sooty yellow and blue flamelets cover the whole surface. Fuel concentration

is everywhere sufficient to reach the air zone and burn in the diffusion zone. The hot region provides conditions for soot formation.

9. Extinction

For low fuel mass flow rates, the fuel is diluted into combustion products and its concentration leaves the flammability limit range, then the flame is extinguished.
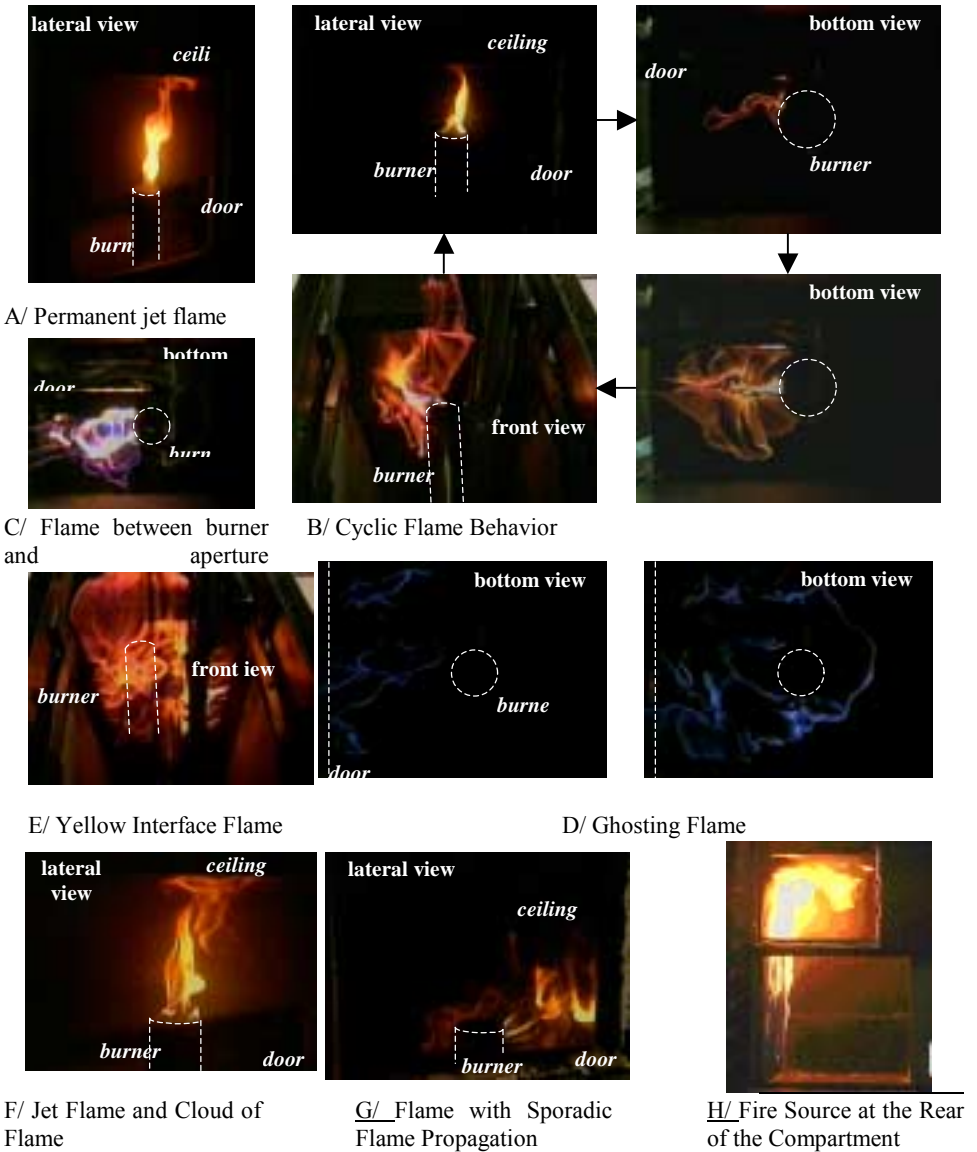

A/ Permanent jet flame

C/ Flame between burner and aperture

B/ Cyclic Flame Behavior

E/ Yellow Interface Flame

D/ Ghosting Flame

F/ Jet Flame and Cloud of Flame

G/ Flame with Sporadic Flame Propagation

H/ Fire Source at the Rear of the Compartment

Fig. 2 : Flame visualisation

A diagram of flame behaviors is given in Fig. 3. Each flame type is represented by a symbol corresponding to $\dot{Q}$ and to the burner position from the soffit bottom (0: soffit level, 1: ceiling level). Similar behaviors are observed with the two soffit heights (Figs. 3.a & 3.b). For low input powers, only jet flames subsist. For higher $\dot{Q}$ values, the flame

persists even for burner positions inside the vitiated region : the flame leaves the burner surface and the hydrocarbon burns in the diffusion zone close to the level of the bottom of the soffit. With $\dot{Q}$, the reaction zone either covers the whole surface (higher $\dot{Q}$), or is intermittent with periodic variations of the heat release rate. The thermal stratification in the enclosure reduces the buoyant convective motion and the reactant mixing. The reaction zone is stretched and the combustion efficiency is dependant of the local fuel-oxygen equivalent ratio leading either to sooty yellow cellular structures or to an unsooty blue flame (ghosting flame). In conclusion, the flame behavior is drastically dependent of both the heat source position and the heat output rate.
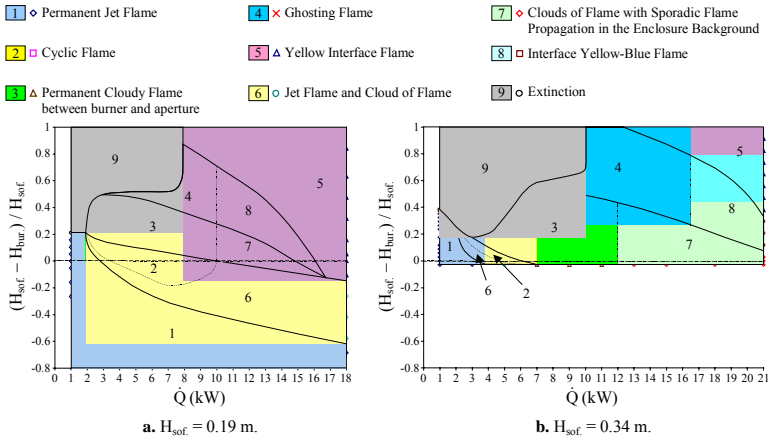
1	◇ Permanent Jet Flame	4	✕ Ghosting Flame	7	◇ Clouds of Flame with Sporadic Flame Propagation in the Enclosure Background
2	□ Cyclic Flame	5	△ Yellow Interface Flame	8	□ Interface Yellow-Blue Flame
3	△ Permanent Cloudy Flame between burner and aperture	6	○ Jet Flame and Cloud of Flame	9	○ Extinction

a. $H_{sof.} = 0.19$ m.   **b.** $H_{sof.} = 0.34$ m.

Fig. 3. Mapping of the flame behavior regions ($X_{bur.} = 0.310$ m and $Z_{bur.} = 0.205$ m).

2/ Simulated Wall Fire at the Rear of the Compartment Lower Part (Fig. 2 H)

The soffit height is 0.19m, the porous burner is installed at the rear of the compartment. For the lower input power ($\dot{Q} = 18\,kW$), a luminous yellow flame is observed along the burner surface and the flame tip hits the ceiling. For upper thermal powers ($\dot{Q} = 45\,kW$), the reacting zone emission is more intense, interacts with the upper vitiated region, a long and thick flame flows down the soffit downward, and leaves the compartment.

AERODYNAMIC CHARACTERIZATION

Outwards Smoke Thickness

For each flame regime, the depth of the hot gas layer, $H_{out\,flow}$, is determined by laser tomography. The occupation rates at the aperture, $H_{out\,flow} / H_{aperture}$, are listed Table 1. The hot smoke layer always occupies 1/3 of the aperture height. These results, in agreement with the Jaluria's observations [13], show that the ventilation of the fire source does not influence the smoke layer thickness at the aperture.

Air Mass Flow Rate Entrained in the Enclosure

The natural ventilation controls the convective motion in the enclosure that induces the air feeding of the flame, hence, the flame behavior. The longitudinal mean velocity, u, of the fresh air entering is measured by LDV.

The results show a symmetry of longitudinal velocity profiles at the room entrance and present an axial plane symmetry. The outward smoke thickness gives the position of the neutral plane (u=0), confirmed by LDV measurements, and is defined as the shear zone between the smoke and the fresh air entering [14]. Input air flow profile is nearly established at the entrance and lateral boundary layers are thin (2D character). This result is verified for all configurations and $u \leq 0.6$ m/s.

The air mass flow rate entering the enclosure, $\dot{m}_{air}$ (Table 1, Fig. 4), is calculated from the longitudinal velocities u integrated on the enclosure width, l, and on the input air height, $H_{in\,flow}$, corresponding to the difference between the aperture height and the

outflow height.
$$\dot{m}_{air}=\int_0^{H_{in\,flow}}\int_0^l \rho\,u\,dy\,dz=\int_0^{H_{in\,flow}}\dot{m}_y\,dy \qquad \text{Eq. 1}$$

The results show that fresh air is mainly entrained in the half lower part of the in flow layer, and the maximum air entrainment rate is observed on the lower third : the flame behavior does not modify the profile of the velocity of the air entering the enclosure.

configuration	case	flame behavior	$\dot{Q}$	$H_{bur.}$	H_{sof}	$\dfrac{H_{out\,flow}}{H_{aperture}}$
Fire source at the rear of the room lower part	A	wall fire	18	/	0.19	0.20
	B	wall fire deflected by ceiling	27	/	0.19	0.27
	C	wall fire deflected by ceiling	36	/	0.19	0.32
	D	wall fire deflected by ceiling	45	/	0.19	0.36
F source in the vitiated upper zone of the room	1	permanent jet flame	3	0.24	0.19	0.30
	2	cyclic flame	5	0.18	0.19	0.32
	3	permanent cloudy flame…	9	0.26	0.34	0.38
	4	ghosting flame	13	0.10	0.34	0.30
	5	yellow interface flame	18	0.13	0.19	0.28
	6	jet flame and cloud of flame	9	0.24	0.19	0.34
	7	clouds of flame…	15	0.33	0.34	0.36
	8	interface yellow-blue flame	11	0.11	0.19	0.26

Table 1. Characteristics and depth of the exit flow of each representative behavior.

The input air mass flow rate in the enclosure is always greater that the fuel/air stoechiometry. For $\dot{Q} \leq 15$ kW, the ratio $H_{out\,flow}/H_{aperture}$ varies between 8 and 13 % for $H_{sof.} = 0.19$ m, and between 14 and 25 % for $H_{sof.} = 0.34$ m. The aperture height (containment level) controls the air mass flow rate entering the enclosure.

The variations of the input mass flow rates are plotted in Fig. 4 for the two soffits. A correlation is obtained (0.19 m soffit height) and fitted by : $\dot{m}_{air}=16.15\,\dot{Q}^{1/3}$ [2] where $\dot{m}_{air}$ is in g.s^{-1} and $\dot{Q}$ in kW. Whatever the characteristics of the heat source (burner surface size, wall or pool fire configurations, position in the enclosure : lower ventilated or upper vitiated zone), the input air mass flow rate is only dependant of the heat release rate power one third (Eq. 2). The input air mass flow rate is independent of the flame behavior (function of type and position of the heat source), but is related both to the source heat release and to the containment level. A relation between input air mass

flow rate, heat release rate and ventilation factor is then sought using an hydrostatic model based on the analysis of Babrauskas'analysis [1].
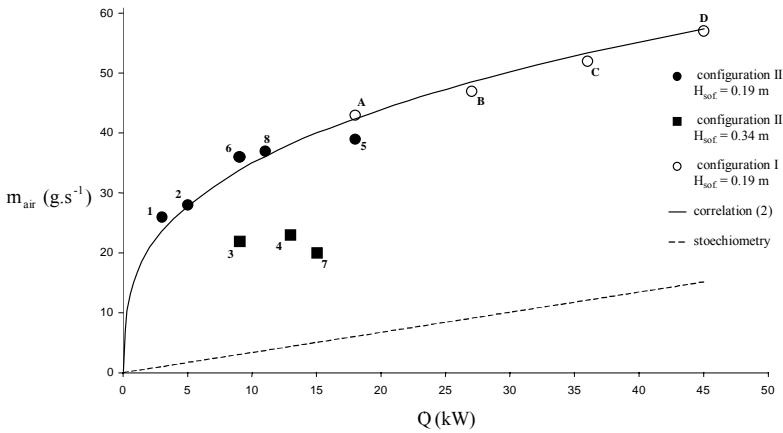

Fig. 4. Measured and stoechimetric input air mass flow rates function of the heat release rate.

Two Zones Hydrostatic Model (Stratified Flow Cases)

The pressure gradient, induced by the thermal expansion of gases, the buoyancy forces and the temperature gradient between in and outside of the room, involves the natural convective fluid motion. Two hydrostatic models for compartment fires are proposed by Karlsson and al [4]). The first one considers an homogeneous and equal smoke concentration and temperature in the room. In the second approach, smoke is only located in the upper zone of the enclosure, thus, internal buoyancy forces are dominant and the flow is stratified. This hypothesis is used to model the two compartment fires.
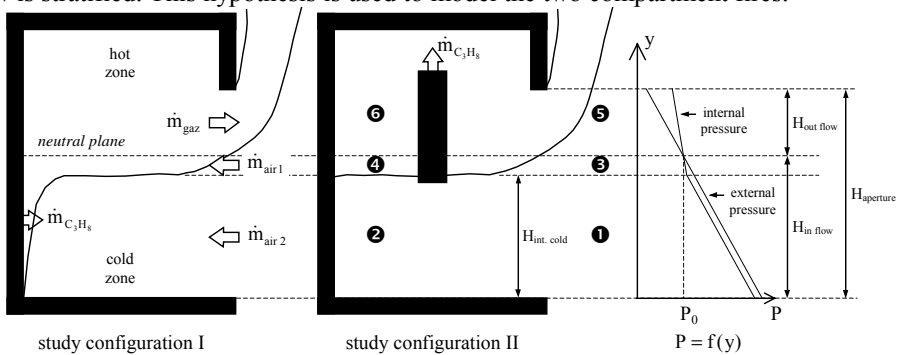

Fig. 5. Two zones hydrostatic model scheme

The two configurations are presented in Fig. 5. to define the stratified flow characteristics. At the neutral plane, the flow velocity is vanished and the pressure, P, corresponds to the atmospheric pressure, P_0. In the enclosure, the smoke layer is thicker than at the aperture under the soffit, the internal cold zone height is defined by $H_{int.\ cold}$.

Mass flow rate at the room aperture is determined from the pressure difference at a y height from the floor. For a given y and from the Bernoulli equation, the kinetic energy of the air (zero initial velocity) is equal to the static pressure variation :

$$\rho \frac{v^2}{2} = \Delta P \qquad\qquad [3]$$

A differential relation of the fluid mass flow rate, $\dot{m}_{fluid}$, flowing through an orifice ('dy' height and 'a' width) with a discharge coefficient C_d is defined from Eq. 3.

$\dot{m}_{fluid} = a\, C_d\, (\rho\, v)\, dy = a\, C_d\, (2\, \rho\, \Delta P)_{1/2} dy$ (with $C_d \cong 0.6$ to 0.8 [14]).   [4]

Considering a two-dimensional flow in the enclosure, the mass flow rate of the hot gases leaving the compartment is obtained from the integration of Eq. 4 on the hot layer thickness under the soffit.

$$\dot{m}_{gaz} = \int_{H_{in\,flow}}^{H_{aperture}} l\; C_d\; (2\, \rho_{hot}\, \Delta P_{65})_{1/2}\, dy \qquad\qquad [5]$$

ΔP_{65} corresponds to the static pressure difference $P_6 - P_5$ between zones ❻ and ❺ at y. P_5, the ambient static pressure at ❺, decreases with y and verifies Eq. 6.

$P_5 = P_0 - \rho_0\, g\, (y - H_{in\,flow}) \qquad\qquad [6]$

As $\rho_{hot} < \rho_0$, the slope of the decrease of P_6 (hot gas static pressure) smaller that P_5 :

$P_6 = P_0 - \rho_{hot}\, g\, (y - H_{in\,flow}) \qquad\qquad [7]$

The introduction of Eqs. 6 and 7 in Eq. 5 leads to Eq. 8 after integration.

$$\dot{m}_{gaz} = \frac{2}{3}\, l\, C_d\, \rho_{hot} \left(\frac{2\, g\, (\rho_0 - \rho_{hot})}{\rho_{hot}} \right)^{1/2} (H_{aperture} - H_{in\,flow})^{3/2} \qquad\qquad [8]$$

A similar approach is used to determine the input air mass flow rate, $\dot{m}_{air\,1}$ between $H_{int.\,cold}$ and $H_{in\,flow}$. P_3 and P_4, the pressures relative to points ❸ and ❹, are respectively equal to $P_0 - \rho_0\, g\, (y - H_{in\,flow})$ and $P_0 - \rho_{hot}\, g\, (y - H_{in\,flow})$ and $\dot{m}_{air\,1}$ verifies:

$$\dot{m}_{air\,1} = \int_{H_{int.\,cold}}^{H_{in\,flow}} l\; C_d\; (2\, \rho_0\, \Delta P_{34})_{1/2} dy = \frac{2}{3}\, l\, C_d\, \rho_0 \left(\frac{2\, g\, (\rho_0 - \rho_{hot})}{\rho_0} \right)^{1/2} (H_{in\,flow} - H_{int.\,cold})^{3/2} \quad [9]$$

The pressure difference between ❶ and ❷ is constant whatever the y height $[\Delta P_{12} = (\rho_0 - \rho_{hot})\, g\, (H_{in\,flow} - H_{int.\,cold})]$, and the air mass flow rate entering in the lower part of the compartment is given by:

$$\dot{m}_{air\,2} = \int_{0}^{H_{int.\,cold}} l\; C_d\; (2\, \rho_0\, \Delta P_{12})_{1/2} dy = l\, C_d\, \rho_0 \left(\frac{2\, g\, (\rho_0 - \rho_{hot})}{\rho_0} \right)^{1/2} (H_{in\,flow} - H_{int.\,cold})^{1/2}\, H_{int.\,cold} \; [10]$$

From Eq. 9 and 10, total air mass flow rate entering the enclosure, $\dot{m}_{air} = \dot{m}_{air\,1} + \dot{m}_{air\,2}$, is:

$$\dot{m}_{air} = \frac{2}{3}\, l\, C_d\, \rho_0 \left(\frac{2\, g\, (\rho_0 - \rho_{hot})}{\rho_0} \right)^{1/2} (H_{in\,flow} - H_{int.\,cold})^{1/2} \left(H_{in\,flow} + \frac{1}{2} H_{int.\,cold} \right) \qquad\qquad [11]$$

An energy balance is written to determine $\dot{m}_{air}$ as a function of $\dot{Q}$. The hydrocarbon is assumed completely consumed within the room, so $\dot{Q}$ is the sum of the heat release rate $\dot{Q}_{exit}$, and of the thermal losses through the walls. $\dot{Q}_{loss}$ is now supposed as negligible: ($\dot{Q}_{loss} = 0$) and gases are considered as perfect; then, the energy balance leads to :

$$\dot{Q} = \dot{Q}_{exit} = \dot{m}_{gaz}\, C_p \left(\frac{\rho_0}{\rho_{hot}} - 1 \right) T_0 \qquad\qquad [12]$$

The incorporation of Eq. 8 in Eq. 12 gives an expression of $\rho_0 - \rho_{hot}$, which, introduced in Eq. 11, leads to Eq. 13.

$$\dot{m}_{air}=\left(\frac{2}{3}\,l\,C_d\right)^{2/3}\left(\frac{2\,g}{C_p}\right)^{1/3}\frac{\rho_0^{1/2}\rho_{hot}^{1/6}}{T_0^{1/3}}\left(\frac{H_{in\,flow}-H_{int.\,cold}}{H_{aperture}-H_{in\,flow}}\right)^{1/2}\left(H_{in\,flow}+\frac{1}{2}H_{int.\,cold}\right)\dot{Q}_{l/3}\quad[13]$$

The mass flow rate ratio, $\dot{m}_{gaz}/\dot{m}_{air}$, is equal to $1+\Phi/r$ for the single chemical reaction:

$$1\,kg\text{ hydrocarbon}+\frac{r}{\Phi}\text{ kg air}\rightarrow\left(1+\frac{r}{\Phi}\right)\text{kg products}\qquad[14]$$
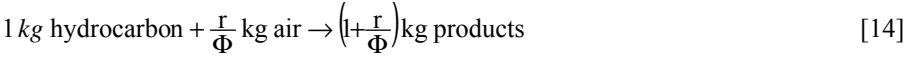
Air entrained in the room is always higher than the stoechiometric value. The hydrocarbon mass flow rate can then be neglected in comparison with the total air mass flow rate, Φ tends to zero and $\dot{m}_{gaz}\approx\dot{m}_{air}$. The equality of Eqs 8 and 13 provides the expression of ρ_{hot} as a function of ρ_0, $H_{aperture}$, $H_{in\,flow}$ and $H_{int.\,cold}$. The expression of ρ_{hot} is now incorporated in Eq. 13, and by introducing the ventilation factor as defined by Kawagoe [6] **:** $F_v=l\,H_{aperture}^{3/2}$, a general air mass flow rate expression is obtained :

$$\dot{m}_{air}=\left(\frac{2}{3}\,C_d\right)^{2/3}\left(\frac{2\,g\,\rho_0^2}{C_p\,T_0}\right)^{1/3}\frac{\left(\frac{H_{in\,flow}}{H_{aperture}}\right)^2}{1-\frac{H_{in\,flow}}{H_{aperture}}}\left(1-\frac{H_{int.\,cold}}{H_{in\,flow}}\right)^{2/3}\left(1+\frac{1}{2}\frac{H_{int.\,cold}}{H_{in\,flow}}\right)^{4/3}F_v^{2/3}\,\dot{Q}_{l/3}\qquad[15]$$

The constant C_1 of $\dot{m}_{air}$ gathers together all the constants. C_2 is function of the heights taken into account by the model. The neutral plane is always supposed at the upper third of the aperture, the $H_{in\,flow}/H_{aperture}$ ratio is then constant and equal to 2/3. From the common character of the linear mass flow rate measured on $H_{in\,flow}$, flows are supposed similar and $H_{int.\,cold}/H_{in\,flow}$ stays constant. Consequently, C_2 is also a constant and Eq. 15 is reduced to Eq. 16 where C is a constant :

$$\dot{m}_{air}=C\,F_v^{2/3}\,\dot{Q}^{1/3}\qquad[16]$$

Quintiere [15] and Steckler [16] have determined $\dot{m}_{air}$ for large scale compartments ($2.8 \times 2.8 \times 2.18\,m^3$) as a function of $\dot{Q}$ and of the ventilation (door widths and windows heights). A porous burner, supplied with methane, was located on the floor at the room center. Their data, the present ones and the theoretical relation are reported in Fig. 6.

The theoretical relation (Eq. 16) is in relatively good agreement for all configurations (compartment scale, heat source position and aperture shape). A small difference subsists between the values of the present C coefficient and Quintiere and Stecker data fitting. This variation can be attributed to errors on $\dot{m}_{air}$ determination due to diagnostic accuracy, but also, on the one hand to the difference between the theoretical heat release and the effective output power: a part of the heat of reaction is dissipated out of the room, on the other hand, heat release rate is a function of the hydrocarbon combustion efficiency, χ_A [17]. It would be more adequate to use the chemical heat quantity $\dot{Q}_{ch}$ in Eq. 16 ($\dot{Q}_{ch}=\chi_A\dot{Q}$). The gap for C also depends of the insulation of the room. A correction of the thermal losses inside the walls and outside the room and of the combustion efficiency, should be evaluated to determine the effective heat released in the room. Consequently, only empirical correlations of Eq. 16 can be proposed here.
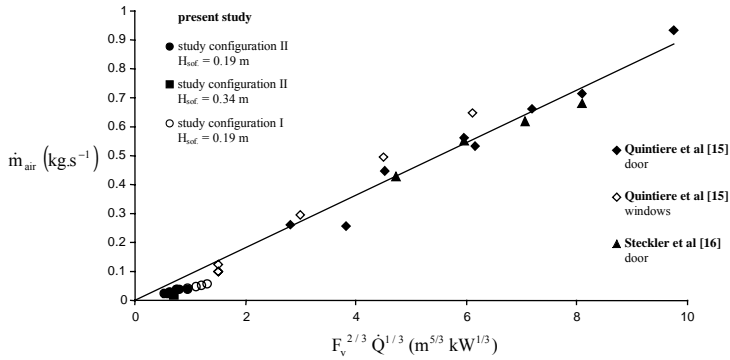
Figure 6. Air mass flow rate as a function of $F_v^{2/3} \dot{Q}^{1/3}$ for different configurations.

In conclusion, the air quantity entrained $\dot{m}_{air}$ into the room is function of the ventilation factor F_v and of the hydrocarbon type, $\dot{m}_{air}$ is independent of the flame type in the room.

CONCLUSION

Two configurations of compartment fires have been studied where the heat source was either a burner located in the vitiated by combustion product upper zone of the enclosure or a simulated wall fire at the rear of the compartment. The influence of the position of the heat source, the heat release rate and the ventilation factor have been determined on the flame behaviors (jet flames, blue, yellow, instable horizontal flames at the room surface, extinction).

Flow aerodynamic has been characterized for each flame regime. The outward hot smoke layer always occupies the top third of the aperture. Based on the analysis of Babrauskas [1], a two zones hydrostatic model has been adapted for the configurations and a relation between the input air mass flow rate entering the room, $\dot{m}_{air}$, the ventilation factor, F_v, and the heat release rate $\dot{Q}$ has been obtained: $\dot{m}_{air} = f(F_v^{2/3} \dot{Q}^{1/3})$. This relation is validated both by the present and full scale experimental data. For a given heat release rate, the air mass flow rate entering the room is function of the ventilation factor but is independent of the flame type in the room.

NOMENCLATURE

$\dot{Q}$:	heat release rate (kW)	u	longitudinal velocity $(m.s^{-1})$
$\dot{m}$	mass flow rate $(kg.s^{-1})$	$\dot{m}_y'$	linear mass flow $(kg.m^{-1}.s^{-1})$
F_v	ventilation factor $(m^{5/2})$	P	pressure (Pa)
B	mass transfer number	ΔP	pressure variation (Pa)
X, Y, Z	spatial coordinates (m)	C_d	discharge coefficient
H	height (m)	g	acceleration due to gravity $(m.s^{-2})$
l	enclosure width (m)	T	temperature (K)
ρ	density $(kg.m^{-3})$	C_p	specific heat $(J.kg^{-1}.K^{-1})$

Φ	correction factor due to air excess	hot	hot zone conditions
r	stoechiometric ratio	0	ambient conditions
C	constant $(kg.s^{-1}.m^{-5/3}.kW^{-1/3})$	int. cold	internal cold zone
χ_A	combustion efficiency	ch	chemical
in&out flow	entering & exiting gas		

REFERENCES

[1] Babrauskas, V., and Williamson, R. B., Post flashover compartment fires: basis of a theoretical model, Fire and Materials, 2, pp. 39-53, 1978.

[2] Babrauskas, V. and Grayson, S.J., Heat release in fires, Elsevier Applied Science, London, 1992.

[3] Drysdale, D., An introduction to fire dynamics, John Wiley and Sons, 2nd Edition, New York, 1999.

[4] Karlsson, B., and Quintiere, J.G., Enclosure fire dynamics, CRC Press, Boca Raton, 2000.

[5] Thomas, P.H., Fires and flashover in rooms - a simplified theory, Fire Safety Journal, 3, pp. 67-76, 1980/81.

[6] Kawagoe, K., Fire behavior in rooms, Building Research Institute, Report n°27, Ministry of Construction, Tokyo, Japan, 1958.

[7] Quintiere, J.G., McCaffrey, B.J. and Den Braven, K., Experimental and theoretical analysis of quasi-steady small-scale enclosure fires, 17th Symp. (Intl.) on Combustion, Leeds, UK, pp. 1125-1137, 1978.

[8] Gross, D., and Robertson, A.F., Experimental fires in enclosures, 10th Symp. (Intl) on Combustion, Cambridge, UK, pp. 931-942, 1964.

[9] Dembsey, N.A., Pagni, P.J. and Williamson, R.B., Compartment fire near-field entrainment measurements, Fire Safety Journal, 24, pp. 383-419, 1995.

[10] de Ris, J., The role of buoyancy direction and radiation in turbulent diffusion flames on surfaces, 15th Symp. (Intl.) on Combustion, pp. 175-182, 1975.

[11] Most, J.M., Sztal, B. and Delichatsios, M.A., Turbulent wall fires : LDV and temperature measurement and implications, 2nd Intl Symp. on Applications of Laser Anemometry to Fluid Mechanic, Lisboa, Portugal, 1984.

[12] Coutin, M., Gautier, B. and Most, J.M., Behavior of the combustion of a fuel material in the vitiated upper zone of an open compartment, 3rd Intl. Seminar on Fire and Explosion Hazards, Preston, UK, 2000.

[13] Jaluria, Y., Natural convection wall flows, SFPE Handbook of Fire Protection Engineering, 1st. Ed, Ch. 1-7, Society of Fire Protection Engineering, Boston, MA, USA., 1988.

[14] Rockett, J. A., Fire induced gas flow in an enclosure, Comb. Sc. and Tech, vol. 12, pp. 165-175, 1976.

[15] Quintiere, J., Rinkinen, W. J. and Jones, W. W., The effect of room openings on fire plume entrainment, Comb. Sc. and Tech., vol. 26, pp. 193-201, 1981.

[16] Steckler, K. D., Quintiere, J. G. and Rinkinen, W. J., Flow induced by fire in a compartment, 19th Symp. (Intl.) on Combustion, pp. 913-920, 1982.

[17] Coutin, M., Most, J.M., Delichatsios, M.A. and Delichatsios, M.M., Flame heights in wall fire: effects of width, confinement and pyrolysis length, 6th Intl. Symp. on Fire Safety Science, Poitiers, France, 1999.